Micromechanics of Material-Removal Mechanisms from Brittle Surfaces: Subsurface Damage and Surface Microroughness

The cold processing of optical glasses usually involves rough grinding, microgrinding, and polishing. In microgrinding,[1,2] the resulting brittle-material-removal rate produces a cracked layer near the glass surface, referred to as subsurface damage (SSD). [Editor's note: The acronym for subsurface damage (SSD) used in this article should not be confused with its more common use as an acronym for smoothing by spectral dispersion.] Of course, the optical quality as well as the strength of the resulting surface is affected by such subsurface damage, so there is the need to understand the generation of subsurface damage as well as its measurement. Preston[3] was the first to observe that the damaged layer usually increases in proportion to the surface microroughness (SR). Preston measured a proportionality factor of 3 to 4, which seemed to be independent of the grinding conditions. We emphasize that subsurface damage is a statistical measure of the ground surface rather than a reflection of the deepest flaw that might control, say, the mechanical strength of the surface.

The direct measurement of SSD is tedious; therefore, fast and reliable techniques to measure subsurface damage are necessary: The dimple method, which is often used,[4,5] relies on the observation that a sufficiently deep spherical impression produced on the damaged optical surface must penetrate into and past the damaged layer. Wafering methods may also be used. The fact that SSD scales with SR was later confirmed, for example, by Aleinikov,[6] who showed that SSD induced by lapping of glasses and other brittle ceramics (with hardness changing 30-fold, fracture toughness 6-fold, and Young's modulus 20-fold) was 3.9±0.2 times SR for SiC abrasives (100 to 150 μm). This observation indicates that SSD may be estimated from SR, whose measurement is significantly simpler and less time consuming. Aleinikov also found that SSD increased with increasing size of microindentation cracks. Aleinikov's correlations between indentation crack length, subsurface damage, and surface roughness are summarized in Fig. 74.64.

Since the Preston[3] and Aleinikov[6] work showed the scaling of SSD with SR under loose-abrasive grinding conditions, it is interesting to extend their observations to bound-abrasive grinding. This issue was more recently examined by Edwards and Hed,[8] who studied the relation of SSD to SR under bound-diamond-abrasive conditions (53 to 65 μm and 180 to 250 μm in size). Edwards and Hed found that for the three glasses they studied (borosilicate crown BK7, zerodur, and fused silica) the average SSD exceeded the proportionality factor of about 4 found under loose-abrasive conditions: Specifically, they found that the average SSD was 6.4±1.3 times the peak-to-valley (p–v) surface roughness (as measured by a profilometer). The factor of 6.4 was arrived at by dividing SSD by SR for each glass. On the other hand, this proportionality factor becomes identical to that of Aleinikov when all three materials tested by Edwards and Hed are treated together (see Fig. 74.65). Similar observations have been reported for deterministic microgrinding of optical glasses with bound-abrasive-diamond tools of smaller size (2 to 4 μm to 70 to 80 μm) (see Lambropoulos *et al.*[9,10]).

In this article, we describe measurements of subsurface damage and surface roughness resulting from microgrinding optical glasses with metal-bonded diamond-abrasive ring tools and present a model for interpreting such data.

Experiments

To study the relation between surface microroughness (SR) and subsurface damage (SSD) in optical glasses, we selected eight glasses that are often used in optical design. The glasses included fused silica (Corning 7940), the borosilicate crown glass BK7, the crown glass K7, the lanthanum crown glass LaK9, the PbO containing dense flint glasses (SF7, SF58), the flint glass F7, the short (kurz) flint glass KzF6, and the dense tantalum flint glass TaFD5.

1. Glass Mechanical Properties

Glasses, like other brittle materials, are characterized by their hardness and fracture toughness.[11,12] Hardness was determined in air via the usual Vickers indentation method with loads ranging from 10 gf to 1 kgf. Fracture toughness was also determined from microindentation, via the model of Evans,[13] which, as we had previously shown,[9] is in good agreement with

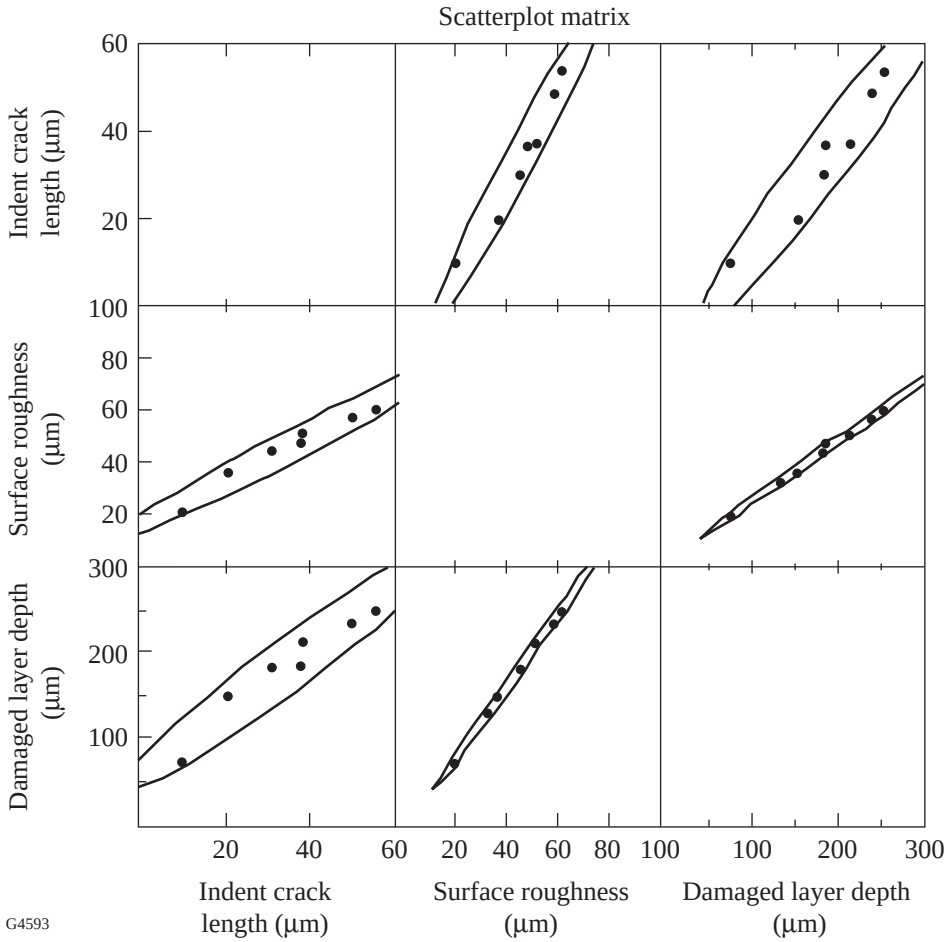

Figure 74.64
Correlations of indentation crack size, surface roughness, and subsurface damage under loose-abrasive conditions. Data are from Aleinikov.[6] Equivalents to Russian glasses can be found in Ref. 7. The individual brittle materials studied by Aleinikov are indicated in the work by Lambropoulos *et al.*[10]

the measurement of fracture toughness via bulk methods. Evans[13] used dimensional analysis and curve fitting over a range of $c/(D/2)$ from 1.5 to 7 and proposed

$$K_c = H\sqrt{D/2}\left(\frac{\mathrm{E}}{H}\right)^{0.4} 10^{f(x)}, \quad x = \log_{10}\left(\frac{c}{D/2}\right),$$
$$f(x) = -1.59 - 0.34x - 2.02x^2 + 11.23x^3 - 24.97x^4 + 16.32x^5, \tag{1}$$

where K_c is fracture toughness, H hardness (Vickers), D indentation diagonal, E Young's modulus, and c the half-crack size. Microindentation of densifying glasses, such as fused silica, cannot be analyzed in this manner.[14–16]

In our notation, H denotes hardness, or resistance to plastic, irreversible deformation, measured by estimating the area of an indentation impressed under load P. Hardness is defined in terms of either projected area or actual area of contact.

Specifically, H_K denotes Knoop hardness, extracted from measuring the long diagonal of a rhomboidal pyramid impression under load P by P/(projected contact area) = (constant) P/(long diagonal)^2, with the (constant) dependent on the rhomboidal pyramid geometry.

H_V denotes Vickers indentation, extracted from measuring the average diagonal of a square pyramid impression under load P by P/(actual contact area) = (constant) P/(average diagonal)^2, with the (constant) dependent on the square pyramid geometry.

For the same measured diagonal, Knoop indentations penetrate about half as much into the surface as Vickers indentations; thus, H_K more closely measures near-surface hardness. Generally, Knoop hardness H_K increases with Vickers hardness H_V. This correlation has been described in detail by Lambropoulos *et al.*[9]

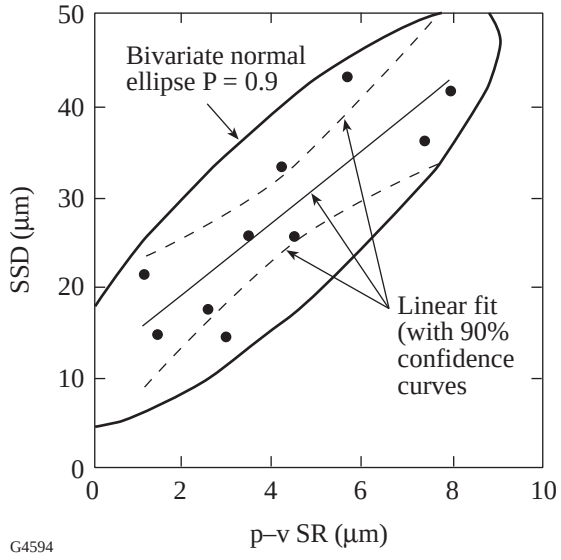

Figure 74.65
Relation of subsurface damage (SSD) to surface roughness (SR), measured in bound-diamond-abrasive grinding by Edwards and Hed.[8] Shown are the bivariate ellipse (at P = 90%, with aspect ratio of about 3.8) and the confidence curves at the level of 90% (dashed line). The straight line fit has a slope of 4.0±0.9 and an intercept of 11±4.

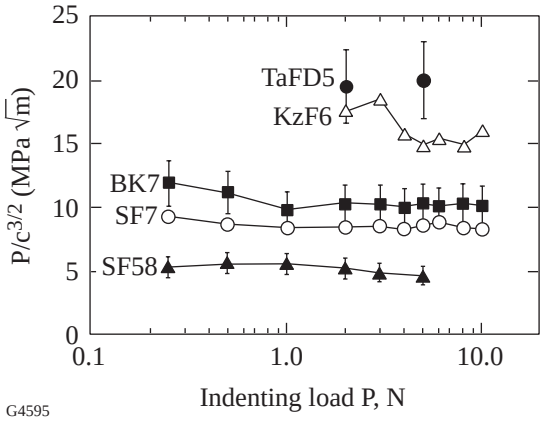

Figure 74.66
Correlation of the measured indentation crack length c (tip-to-tip surface trace length is 2c) with applied load P shows essentially a constant value of the ratio $P/c^{3/2}$.

Figure 74.66 shows the measured values of $P/c^{3/2}$ versus the applied load P for some of our tested glasses, indicating that this ratio is essentially constant over the indenting loads used. Table 74.IV shows the glass thermomechanical properties. Data for density ρ, glass transition temperature T_g, coefficient of thermal expansion α, Young's modulus E, and Poisson ratio ν are from manufacturers' catalogs. Knoop hardness H_K and Vickers hardness H_V are at 1.96 N. K_c for fused silica was taken from the Corning catalog. H_V and K_c data of LaK9 were estimated from that of neighboring glasses LaK10, LaK11.[9,17] Data in Table 74.IV other than Vickers hardness have been reported previously.[10]

2. Deterministic Microgrinding Experiments

The surface-grinding experiments were done on a deterministic microgrinding platform, where infeed rate is imposed, thus resulting in surfaces of minimal figure errors, superior finish, and minimal damage. Imposing infeed rate leads to precise knowledge of the amount of removed material when microgrinding optical glasses. In the platform used, both the tool and work axis spin. The variable angle between these axes of rotation can be used to produce spherical surfaces of variable radius of curvature (from 5 mm to planar surfaces).

Table 74.IV: Thermomechanical properties of optical glasses.

Glass	ρ g/cm^3	T_g °C	α $10^{-6\circ}$ C^{-1}	E GPa	ν	H_K GPa	H_V GPa	K_c MPa $\sqrt{m}$
FS-C7940	2.20	1,090	0.52	73	0.17	5.6	8.5	0.75
SF58	5.51	422	9.0	52	0.26	2.7	3.5	0.46
SF7	3.80	448	7.9	56	0.23	3.4	5.3	0.67
BK7	2.51	559	7.1	81	0.21	5.1	7.2	0.82
K7	2.53	513	8.4	69	0.21	4.6	6.2	0.95
KzF6	2.54	444	5.5	52	0.21	3.7	5.5	1.03
LaK9	3.51	650	6.3	110	0.29	5.7	(5.5)	(0.95)
TaFD5	4.92	670	7.9	126	0.30	7.3	10.0	1.54

Pollicove and Moore have described progress in fabrication of precision optical components via deterministic microgrinding with rigid, computer-controlled machining centers and high-speed tool spindles.[18,19] Deterministic microgrinding has been used to manufacture convex and concave spherical surfaces, as well as aspheres. Specular surfaces, resulting after less than 5 min of deterministic microgrinding, have typical rms microroughness of less than 20 nm, 1 μm of subsurface damage, and a surface figure better than 1/2 wave peak-to-valley. Typical infeed rates are 5 to 10 μm/min with 2- to 4-μm bound-abrasive-diamond tools.

Three metal-bonded diamond-abrasive ring tools were sequentially used on each surface (aqueous coolant Loh K-40, relative speed of work and tool of about 30 m/s): 70 to 80 μm, 10 to 20 μm, and 2 to 4 μm at infeed rates of 1 mm/min, 50 μm/min, and 5 μm/min, respectively. Three cuts were done with each tool, all at a tool speed of about 30 m/s (tool rotation of 11,250 rpm, work rotation of 150 rpm).

After each cut, the surface roughness (SR) at three locations on the optical surface was measured using the Zygo New View 100 white-light interferometer (20× Mirau), a 3-D imaging surface structure analyzer. It uses coherence-scanning white-light interferometry for noncontact imaging and measurement of surface microstructure and topography. One portion of a light beam reflects from a test surface and the other portion from an internal high-quality reference surface. Both portions are then directed onto a solid-state camera with 320 × 240 pixels. Interference between the two light-wave fronts results in an image of light and dark interference fringes, indicating the surface structure of the test part. The test part is scanned by vertically moving the objective with a piezoelectric transducer. As the objective scans, a video system captures intensities at each camera pixel. Lateral resolution is determined by the microscope objective field of view and the number of pixels and is ultimately limited by the wavelength of the light source. With a 20× objective, the field of view is 0.35×0.26 mm^2.

Subsurface damage (SSD) was measured with the dimple method,[4,5] in which a steel ball is gently ground with fine diamond paste (0.25 μm) onto the optical surface, thus penetrating into and past the SSD zone. Optical measurement of the image reveals an outer ring of SSD surrounding an inner circle of damage-free surface. Measurement of the ring radii and knowledge of the steel sphere radius lead to the extraction of the SSD. Three dimples were done for each cut for the 2- to 4- and 10- to 20-μm tools. Because of the time required to produce dimples into and past the SSD of the surfaces ground with the 70 to 80 abrasives, no SSD measurements were done on these surfaces. Figures 74.67 and 74.68 summarize the roughness and subsurface damage measurements.

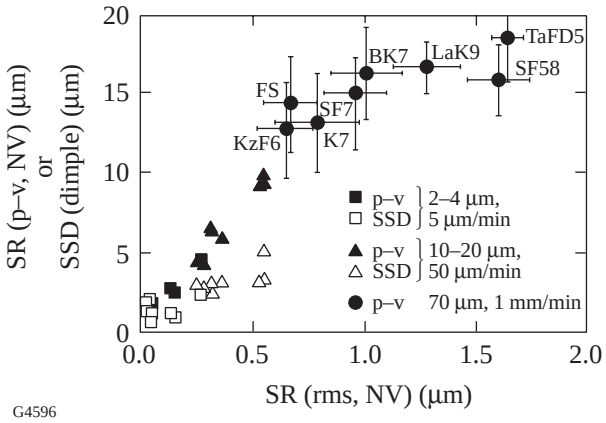

Figure 74.67
Summary of the measurements of peak-to-valley and rms surface roughness (SR) resulting from all three grinding tools used. Surface roughness was measured via the New View white-light interferometer, and subsurface damage (SSD) via the dimple method.

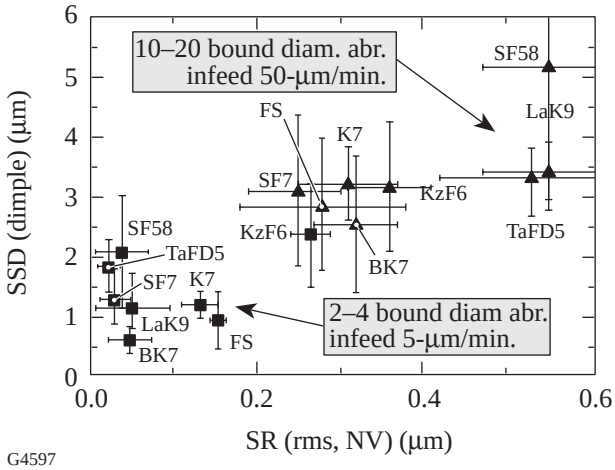

Figure 74.68
Summary of measurements for the rms surface roughness (SR) (white-light interferometry) and subsurface damage (SSD) (dimple method) for the deterministically microground surfaces with the 2- to 4-μm and 10- to 20-μm abrasives. A straight line correlation of all data has a slope of 5.5±0.9 and $R^2 = 0.73$.

Model for Ratio of Subsurface Damage to Surface Roughness

When a sharp indenter transmits normal load P into a brittle surface, the resulting indentation diagonal D is determined by the force P, the material hardness, and the sharpness of the indenting surface:

$$H = \frac{2P\sin\psi}{D^2} \tag{2}$$

with hardness defined via contact area between the indenter and the material (Fig. 74.69). Indentation mechanics can be simplified by considering the displaced material as occupying the volume of an equivalent half-sphere of radius a. Equating the volume displaced under the actual indenter (diagonal D) with that of the equivalent half-sphere volume $2\pi a^3/3$, we find

$$\frac{a}{D} = \left[\frac{3}{24\pi\sqrt{2}}\right]^{1/3}(\cot\psi)^{1/3} = 0.304(\cot\psi)^{1/3}. \tag{3}$$

Indentation induces a larger zone of plastically deformed material, approximately hemispherical with radius b. Length scales a (radius of indented half-sphere) and b (plastic zone size) can be correlated via the Hill model of the expanding cavity in a perfectly plastic material, discussed by Chiang *et al*.[20] This relation is further simplified to[20,21]

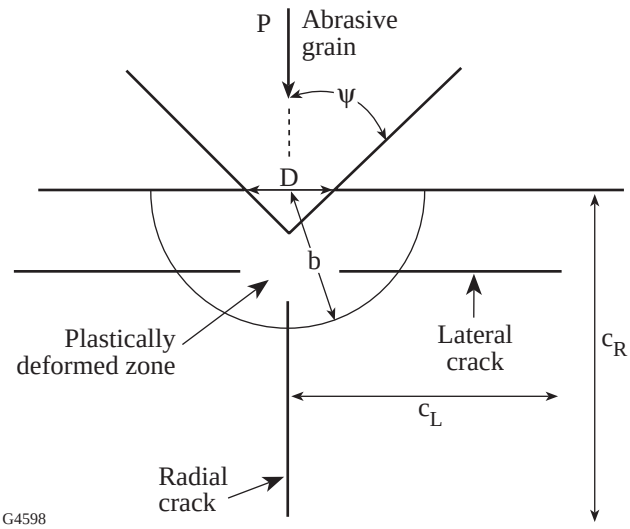

Figure 74.69
Schematic of sharp indentation shows indentation diagonal D, plastic zone size b, lateral and radial crack lengths c_L and c_R. Volume displaced by the indenter is equivalent to half-sphere of radius a.

$$\frac{b}{a} = \left(\frac{E}{H}\right)^m, \tag{4}$$

where m is a dimensionless constant in the range $m = 1/3$ to 1/2. The more traditional approach in the fracture literature uses $m = 1/2$.[22–24] More recent data analysis suggests that $m = 1/3$ may be more appropriate.[25]

When the load P exceeds some threshold value, surface cracks appear.[21] The length c_R of radial cracks emanating from the indentation is related to fracture toughness K_c and load P by[22–25]

$$K_c = \alpha_K\left(\frac{E}{H}\right)^{1-m}(\cot\psi)^{2/3}\frac{P}{c_R^{3/2}}. \tag{5}$$

α_K is a dimensionless number, found from indentation data of Fig. 74.66 for the three glasses TaFD5 (high fracture toughness K_c), BK7 (intermediate K_c), and SF58 (low K_c). We fitted Eq. (5) to the measured fracture toughness K_c for $m = 1/2$ and $m = 1/3$, and found

$$\alpha_K(m) = 0.027 + 0.090\left(m - \frac{1}{3}\right). \tag{6}$$

Fracture mechanics analysis of microindentation shows that the residual stress field is tensile at the boundary of the elastic and plastic zones at the symmetry axis of the indentation, where any lateral cracking is expected to originate.[21,26] As lateral cracks remove material from the surface, we assume that the resulting SR is equal to the plastic zone depth b, following Buijs and Korpel–Van Houten.[27,28] Other assumptions may also be made, as by Lambropoulos *et al*.[29] Such assumptions have been compared and discussed by Lambropoulos.[30] We also assume that the depth SSD of the subsurface damage zone is equal to the depth of the radial cracks c_R; thus, the ratio of SSD to SR is

$$\frac{\text{SSD}}{\text{SR}} = \frac{c_R}{b} = 2.326\,\alpha_K^{2/3}\left(\frac{E}{H}\right)^{(2-5m)/3}$$

$$\frac{(\cot\psi)^{1/9}}{(\sin\psi)^{1/2}}\left[\frac{P}{\left(K_c^4/H^3\right)}\right]^{1/6}. \tag{7}$$

Indenting load P naturally scales with the material length scale K_c^4/H^3, as has been observed previously by Lawn,[31,32] Chiang *et al*.,[21] and Marshall *et al*.[26] The dependence of the ratio SSD/SR on the actual load P is rather weak (power of 1/6), which explains the experimental fact that over a wide range of abrasives, speeds, and pressures used there seems to be a constant ratio of SSD to SR (for example, Refs. 6 and 8).

Figure 74.70 shows the dependence of the SSD/SR on load P and sharpness angle ψ. For sharp abrasives ($\psi \to 0$), the ratio SSD/SR $\to \infty$, whereas for flat abrasives $(\psi \to \pi/2)$, SSD/SR $\to 0$. Figure 74.71 shows that by using typical material properties for optical glasses, intermediate values of ψ(20° to 80°), and typical indenting loads from 0.1 to 10 N, the ratio SSD/SR is in the range 4±2. Our range of indenting loads includes loads estimated to occur under lapping conditions. Chauhan *et al*.[33] estimated the maximum transmitted force to vary from 1.2 to 4.1 N as lapping abrasives ranged in size from 10 to 65 μm.

Guided by the model predictions for the dependence of ratio SSD/SR on glass mechanical properties, we have plotted in Fig. 74.72 the measured ratio SSD/SR versus the factor K_c^4/H^3 for grinding with the 10 to 20 abrasives under deterministic micro-grinding conditions (data from Fig. 74.68). Plotted in this manner, the experimental data show a dependence on K_c^4/H^3 like a power of –0.15±0.08, which is in general agreement with the model predictions of a power of –0.167. Of course, such a comparison is valid only as long as the force transmitted by the bonded abrasive grains is essentially constant among the various ground glasses.

The model discussed above also allows us to address the question: Under what circumstances can the depth of subsurface damage actually be less than the surface roughness? Such a condition would essentially mean that no subsurface damage would be present in the ground surface, thus resembling a condition of ductile grinding or polishing. Requiring that ratio SSD/SR < 1 leads to

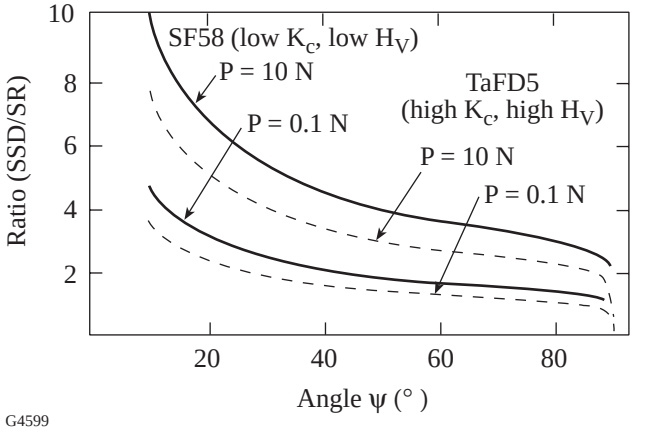

Figure 74.70
Ratio SSD/SR versus sharpness angle ψ for properties corresponding to glasses TaFD5 (hard, tough) and SF58 (soft, brittle). Indenting forces 0.1 or 10 N; factor $m = 0.40$.

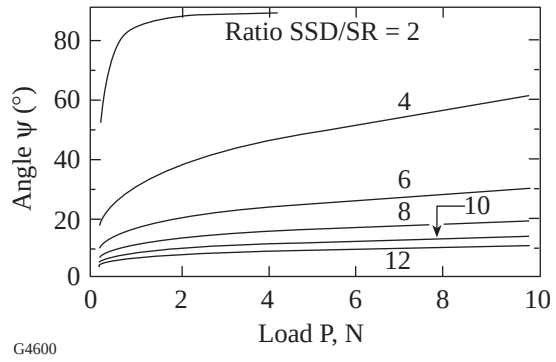

Figure 74.71
Ratio SSD/SR versus sharpness angle ψ and load P for typical optical glass (BK7). Factor $m = 0.40$.

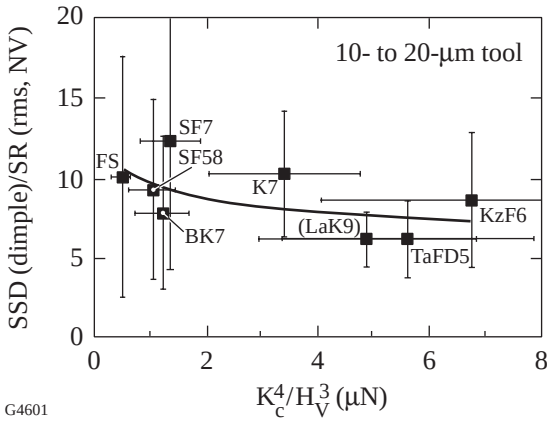

Figure 74.72
Measured ratio of subsurface damage (dimple method) to rms surface roughness (interferometry) versus the material-dependent load K_c^4/H^3 for the surfaces ground with the 10- to 20-μm metal-bonded diamond-abrasive tools. Hardness is H_V at 1.96 N. Datum for LaK9 is in parentheses since its K_c and H_V were estimated from neighboring glasses LaK10 and LaK11.

$$\frac{\mathrm{SSD}}{\mathrm{SR}} < 1 \Rightarrow P < \frac{\left(K_c^4/H^3\right)}{(2.326)^6\ \alpha_K^4 \left(\dfrac{\mathrm{E}}{H}\right)^{2(2-5m)}} \frac{(\sin\psi)^3}{(\cot\psi)^{2/3}}. \quad (8)$$

This result reveals that in order to promote more polishing-like conditions, the right-hand side of the above inequality must be made as large as possible to accommodate as large as possible a range of indenting forces P. Noticing that the dependence on the ratio (E/H) is rather weak (since m is in the range from 1/3 to 1/2), the polishing-like conditions can be achieved by a large value of the material-dependent load scale K_c^4/H^3, or by a large value of the angular factor $(\sin\psi)^3/(\cot\psi)^{2/3}$. This factor is a monotonically increasing function of the abrasive sharpness ψ; thus, polishing-like conditions are promoted by high fracture toughness K_c, low hardness H, and relatively flat abrasives contacting the manufactured optical surface. These effects are in addition to the chemical effects identified by Cook.[34] Notice, however, that other mechanical effects in polishing have been identified, both for polishing with traditional methods such as polyurethane pads[35,36] and for more recent polishing platforms that take advantage of subaperture material removal under computer–numerically controlled algorithms where the polishing slurry is a mixture of abrasive particles with a magnetorheological fluid, as discussed by Jacobs *et al.*[37] and interpreted by Lambropoulos *et al.*[38]

Figure 74.67 shows that for those instances where both the p–v roughness and the subsurface damage (SSD) were measured, the p–v roughness was an upper bound to the subsurface damage. For the finer 2- to 4-μm bonded diamond abrasives, the measured p–v roughness is a good approximation to the actual SSD. For the intermediate 10- to 20-μm abrasives, the p–v roughness is a close upper approximation to the SSD. The reason is that the dimple method reveals a statistical measure of subsurface damage, without being able to identify the deepest flaw. On the other hand, the p–v roughness is dictated by the single deepest flaw detected within the measured area. Thus, we expect that the p–v roughness would exceed the SSD measurement by the dimple method, as indeed our measurements indicate. The usefulness of this observation becomes clear from the fact that, when the subsurface damage from a very rough ground surface is to be determined, the dimple method must produce a dimple into and past the damaged zone. This would be a very time-consuming and labor-intensive task for deep SSD, while requiring only a few minutes when subsurface damage is only a few microns in depth.

Conclusions

We have presented a micromechanics model based on the sharp indentation of a brittle surface to interpret the measured ratio of subsurface damage (SSD) to surface microroughness (SR). The measurements were done under deterministic microgrinding conditions where the imposed infeed rate produces surfaces with minimal figure error, and optimum surface roughness and subsurface damage. The glasses ground span a wide range of optical glasses.

We used 70- to 80-μm, 10- to 20-μm, and 2- to 4-μm abrasives at infeeds of 1 mm/min, 50 μm/min, and 5 μm/min, respectively. For the 70- to 80-μm abrasives, the rms SR, measured with white-light interferometry, ranges from 0.65 to 1.6 μm and the p–v roughness from 12 to 19 μm. For the 10- to 20-μm abrasives, rms SR ranges from 0.25 to 0.55 μm, p–v from 4 to 10 μm, and the SSD (measured with the dimple method) from 2.5 to 5.1 μm. For the 2- to 4-μm abrasives, rms SR ranges from 0.02 to 0.27 μm, p–v from 1.3 to 4.4 μm, and the SSD (measured with the dimple method) from 0.90 to 2.3 μm.

These measurements support the conclusion that peak-to-valley surface roughness measured by interferometry provides an upper bound to the subsurface damage measured via the dimple method. This observation is useful, and its applicability should be further explored for a wider range of optical materials under a large range of manufacturing processing conditions.

The micromechanics model predicts the ratio of SSD/SR in terms of the load transmitted by the abrasive grain, the sharpness of the abrasive, and the glass mechanical properties (Young's modulus E, hardness H, fracture toughness K_c). The dependence on load is rather weak, in agreement with our measurements and others. The effect of abrasive sharpness is more pronounced. In the limit of SSD/SR < 1, i.e., when polishing-like or ductile grinding conditions prevail, no SSD can be identified because it is enveloped within the surface microroughness. Such conditions are promoted for brittle materials with high fracture toughness and low hardness. Flat abrasive grains have the same effect.

ACKNOWLEDGMENT

We acknowledge many helpful discussions with and insights from Mr. Don Golini of QED Technologies, LLC (Rochester, NY) and with Profs Paul Funkenbusch, Stephen Burns, and James C. M. Li of the Mechanical Engineering Department at the University of Rochester.

REFERENCES

1. T. S. Izumitani, *Optical Glass*, American Institute of Physics Translation Series (American Institute of Physics, New York, 1986), Chap. 4, pp. 91–146.
2. H. H. Karow, *Fabrication Methods for Precision Optics* (Wiley, New York, 1993), Chap. 5.
3. F. W. Preston, Trans. Opt. Soc. **XXIII**, 141 (1921–22).
4. A. Lindquist, S. D. Jacobs, and A. Feltz, in *Science of Optical Finishing*, 1990 Technical Digest Series (Optical Society of America, Washington, DC, 1990), Vol. 9, pp. 57–60.
5. Y. Zhou *et al.*, J. Am. Ceram. Soc. **77**, 3277 (1994).
6. F. K. Aleinikov, Sov. Phys. Tech. Phys. **27**, 2529 (1957).
7. L. B. Glebov and M. N. Tolstoi, in *CRC Handbook of Laser Science and Technology*, Vol. V: Optical Materials, Part 3, Supplement 2: Optical Materials, edited by M. J. Weber (CRC Press, Boca Raton, FL, 1995), pp. 823–826.
8. D. F. Edwards and P. P. Hed, Appl. Opt. **26**, 4677 (1987).
9. J. C. Lambropoulos, T. Fang, P. D. Funkenbusch, S. D. Jacobs, M. J. Cumbo, and D. Golini, Appl. Opt. **35**, 4448 (1996).
10. J. C. Lambropoulos, S. D. Jacobs, B. Gillman, F. Yang, and J. Ruckman, in *Advances in Fusion and Processing of Glass II*, edited by A. G. Clare and L. E. Jones, Ceramic Transactions, Vol. 82 (The American Ceramic Society, Westerville, OH, 1998), pp. 469–474. See also Laboratory for Laser Energetics LLE Review **73**, 45, NTIS document No. DOE/SF/19460-212 (1997). Copies may be obtained from the National Technical Information Service, Springfield, VA 22161.
11. R. F. Cook and G. M. Pharr, J. Am. Ceram. Soc. **73**, 787 (1990).
12. I. J. McColm, *Ceramic Hardness* (Plenum Press, New York, 1990).
13. A. G. Evans, in *Fracture Mechanics Applied to Brittle Materials*, edited by S. W. Freiman (American Society for Testing and Materials, Philadelphia, 1979), Vol. ASTM STP 678, Part 2, pp. 112–135.
14. A. Arora *et al.*, J. Non-Cryst. Solids **31**, 415 (1979).
15. H. Li and R. C. Bradt, J. Non-Cryst. Solids **146**, 197 (1992).
16. J. C. Lambropoulos, S. Xu, and T. Fang, J. Am. Ceram. Soc. **79**, 1441 (1996).
17. J. Schulman, T. Fang, and J. Lambropoulos, *Brittleness/Ductility Database for Optical Glasses*, ver. 2.0, Department of Mechanical Engineering and Center for Optics Manufacturing, University of Rochester, Rochester, NY (1996).
18. H. M. Pollicove and D. T. Moore, Laser Focus World, March 1991, 145.
19. H. M. Pollicove and D. T. Moore, in *Optical Fabrication and Testing Workshop Topical Meeting*, 1992 Technical Digest Series (Optical Society of America, Washington, DC, 1992), Vol. 24, pp. 44–47.
20. S. S. Chiang, D. B. Marshall, and A. G. Evans, J. Appl. Phys. **53**, 298 (1982).
21. *ibid.*, 312.
22. A. G. Evans and E. A. Charles, J. Am. Ceram. Soc. **59**, 371 (1976).
23. B. R. Lawn, A. G. Evans, and D. B. Marshall, J. Am. Ceram. Soc. **63**, 574 (1980).
24. G. R. Anstis *et al.*, J. Am. Ceram. Soc. **64**, 533 (1981).
25. M. T. Laugier, J. Mater. Sci. Lett. **4**, 1539 (1985).
26. D. B. Marshall, B. R. Lawn, and A. G. Evans, J. Am. Ceram. Soc. **65**, 561 (1982).
27. M. Buijs and K. Korpel-van Houten, J. Mater. Sci. **28**, 3014 (1993).
28. M. Buijs and K. Korpel-van Houten, Wear **166**, 237 (1993).
29. J. Lambropoulos, M. J. Cumbo, and S. D. Jacobs, in *Optical Fabrication & Testing Workshop Topical Meeting* (Optical Society of America, Washington, DC, 1992), Vol. 24, pp. 50–53.
30. J. C. Lambropoulos, S. Xu, and T. Fang, Appl. Opt. **36**, 1501 (1997).
31. B. R. Lawn, T. Jensen, and A. Arora, J. Mater. Sci. **11**, 573 (1976).
32. B. R. Lawn and D. B. Marshall, J. Am. Ceram. Soc. **62**, 347 (1979).
33. R. Chauhan *et al.*, Wear **162–64**, 246 (1993).
34. L. M. Cook, J. Non-Cryst. Solids **120**, 152 (1990).
35. T. S. Izumitani, in *Workshop on Optical Fabrication and Testing: A Digest of Technical Papers* (Optical Society of America, Washington, DC, 1982), pp. 1–4.
36. J. C. Lambropoulos, in *Optical Fabrication and Testing*, 1996 Technical Digest Series (Optical Society of America, Washington, DC, 1996), Vol. 7, pp. 88–91.
37. S. D. Jacobs, D. Golini, Y. Hsu, B. E. Puchebner, D. Strafford, Wm. I. Kordonski, I. V. Prokhorov, E. Fess, D. Pietrowski, and V. W. Kordonski, in *Optical Fabrication and Testing*, edited by T. Kasai (SPIE, Bellingham, WA, 1995), Vol. 2576, pp. 372–382.
38. J. Lambropoulos, F. Yang, and S. D. Jacobs, in *Optical Fabrication and Testing*, 1996 Technical Digest Series (Optical Society of America, Washington, DC, 1996), Vol. 7, pp. 150–153.